Colloids and Surfaces A: Physicochem. Eng. Aspects 429 (2013) 112–120

Contents lists available at SciVerse ScienceDirect

Colloids and Surfaces A: Physicochemical and Engineering Aspects

journal homepage: www.elsevier.com/locate/colsurfa

Influence of relative humidity and nano-particle concentration on pattern formation and evaporation rate of pinned drying drops of nanofluids

D. Brutin*

Aix-Marseille University, IUSTI UMR 7343 CNRS, 13453 Marseille, France

HIGHLIGHTS

- Relative humidity changes the evaporation rate but not the pattern formation.
- Transition from the coffee ring effect to homogenous deposition is observed.
- The evaporation rate increase with decreasing humidity more than predicted.

GRAPHICAL ABSTRACT

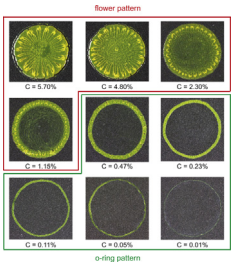

ARTICLE INFO

Article history:
Received 16 November 2012
Received in revised form 18 February 2013
Accepted 6 March 2013
Available online 11 April 2013

Keywords:
Nano-particles
Humidity
Diffusion
Evaporation

ABSTRACT

We report the pattern formation of nano-particles of iso-density water-based nanofluid drops. During the spontaneous evaporation of a droplet in air under atmospheric conditions, the solvent evaporates and nano-particles are deposited onto the substrate. Depending on the concentration, two different patterns are observed: an o-ring pattern and a continuous nano-particle flower pattern. We observe a critical concentration that corresponds to the transition between the two patterns. Humidity is controlled and modified to investigate its effect on the evaporation dynamics and on pattern formation. Surprisingly, the leading pattern is identical regardless of the evaporation time, and the evaporative mass fluxes measured are slightly higher than the expected flux, following a classical purely diffusive model for pure fluids. Two explanations are proposed: the first is that the diffusion coefficient of the nanofluid in humid air is different from that of pure water in dry air. The second is based on the experimental observation of an increase in the spreading of the nanofluid, leading to an increase in the drop perimeter, a decrease in the contact angle and thus an improvement in the evaporation rate.

1. Introduction

While nanofluids are widely studied in several scientific communities (physics, biology, chemistry, etc.), several questions regarding their heat transfer efficiency, stability and toxicity to human health currently remain open problems. One important application for nanofluids is inkjet printing [1], though nanofluids are very promising for tow-phase heat transfer as well [2]. Using metallic nano-particles, inkjet printer technology is evolving to allow for the printing of metallic inks on soft substrates for photovoltaic and several others applications. These metallic inks are mostly made of silver, and consequently, they are very expensive (about $500 per milliliter). To create controlled patterns using inkjet printing technology, a chain of droplets, whose volume has been calculated, must create lines of constant diameter following evaporation. The homogeneity of the line thickness is important because it will affect the electrical resistivity of the resulting pattern. If the concentration of nano-particles is too low, an o-ring pattern will appear, which means that the matter will not have been uniformly deposited on the substrate. If the concentration is too

* Tel.: +33 4 91 10 68 86; fax: +33 4 91 10 69 69.
E-mail address: david.brutin@univ-amu.fr

0927-7757/$ – see front matter © 2013 Elsevier B.V. All rights reserved.
http://dx.doi.org/10.1016/j.colsurfa.2013.03.012

high, then the final thickness will also be too high, exceeding a certain thickness above which the electrical resistivity will no longer change; thus, nano-particles, which are extremely expensive, will have been wasted. Thus, the search for the optimal concentration that avoids o-ring formation and consequently enables a uniform deposition by minimizing the amount of nano-particles is of great interest. Several authors are currently looking at the driving parameters that lead to such pattern formation [3]. However, because the evaporation of even a pure fluid droplet remains a complex topic, there is much research to be done to understand the evaporation of complex fluids [4–6].

O-ring formation during colloidal drop evaporation was first explained by R.D. Deegan in 2000 [9]. By using sulfate-terminated polystyrene spheres of two sizes, 1 and 0.1 μm, at a maximum volume concentration of 2% dried on glass plates, the author observed the formation of different patterns depending on the concentration and size of the spheres used. For spheres measuring 100 nm and concentrations ranging from 0.25% to 0.063%, Deegan observed the formation of multiple rings for initial droplets measuring 6 mm in diameter. In all cases, particles remained at the drop center and were not only located at the drop edge. In this study, we observed two different final patterns depending on the concentration: an o-ring pattern and a nearly uniform deposition pattern on the substrate. Similar results has been observed by Denkov et al. [22] for latex particles. In the case of mixtures of more complex fluids, at low concentrations, the formation of nano-particle rings following the evaporation of droplets was evidenced by Govor et al. in 2004 [11] for a liquid matrix of a binary mixture of nitrocellulose, amyl acetate and hexane. The authors used 6 nm nano-particles of $CoPt_3$ at concentrations below 1%, leading to rings measuring 0.6–1.5 μm in diameter. They experimentally observed the phase separation that leads to the formation of a bilayer structure. The $CoPt_3$ nano-particles located on the contact line assembled along the line. In this case, in which spheres smaller than our nano-particles were used, the accumulation at the drop edge was more pronounced. Conway et al. [7] first investigated the influence of particles on the evaporation dynamics of a drop. Using 200 and 750 nm polystyrene beads, the author observed the formation of an o-ring and a crater for these bead diameters and monitored the drop height and mass over time. Conway et al. provide linear normalized model of the drop mass and normalized model of the drop height using a root square function.

Chhasatia et al. [10] investigated the effect of relative humidity on the contact angle and nano-particle deposition during the evaporation of a pico-liter droplet of a nanofluid. They observed, for the pinned droplet mode, a spreading effect with the increase in relative humidity. The observed variations in the contact angle were linear but exhibited different slopes depending on the relative humidity. The researchers conclude that due to the small volume of the droplet, the relative humidity becomes an important parameter driving the evaporation process and consequently the deposition. They also observed an increase in the initial spreading of the drop with increasing humidity. Chhasatia and Sun [1] used bi-dispersed colloids made of micro- and nano-particles and observed the interaction between these particles and the contact line. For 100 nm and 1.1 μm particles, they observed that, at the end of the evaporation process, the nano-particles were located near the triple line, followed by the micro-particles. This phenomenon is explained by a force balance.

During the drying of droplets containing latex particles measuring 40 nm to 5 μm, Monteux and Lequeux [18] observed a rearrangement that led to the formation of rings. The smallest nano-particles were deposited on the outer side of the ring, while the largest particles were located on the inner side. The authors conclude that this deposition mechanism leads to a tight deposition but leaves a thin liquid film of pure water at the edge of the drop. The deposited particle ring size can be precisely controlled by changing the particle size. The segregation effect may consequently play an important role in polymer and biological fluids, which are composed of poly-disperse particles. Using 100 nm particles, Marin et al. [8] demonstrated that the particles that settle first along the contact line of a coffee ring pattern have an ordered, crystalline structure. Toward the center of the drop, a transition to a disordered particle arrangement was observed.

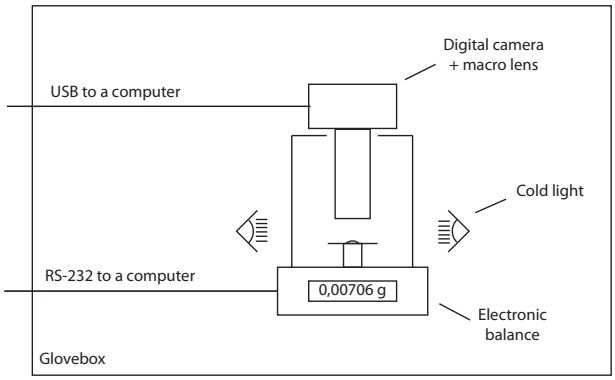

Fig. 1. Schematic of the experiment.

Pattern formation has also been observed for biological fluids, such as whole blood, very recently and shows similar patterns to those of nanofluids [13]. The drying dynamics observed for this complex biological fluid show two typical regimes of drying, with the first one driven by diffusion and convection and the second driven only by diffusion through the dried deposit [14]. Finally, pattern formation is influenced by the wettability of a droplet on a substrate. The relationship between the spreading of a droplet and the evaporation dynamics has been previously discussed [15]. The triple line dynamics and the pinning of a drop play a major role in the drying process. Consequently, the motion of flow inside a drop is also strongly affected, as we have evidenced using infrared imaging [12].

In this study, we used 24-nm-diameter polystyrene sphere at concentrations ranging from 0.01% to 5.70% deposited on a 0.5 mm thick aluminum disk with a diameter of 10 mm coated with a Nuflon 16× coating to enable the pinning of the drops regardless of the surrounding conditions. The humidity was controlled, and the temperature was observed to not affect the evaporation dynamics. Only the effect of the nano-particle concentration on the pattern formation was monitored. The nano-particles used were coated with carboxylate and an acid used as a surfactant to stabilize the particles. The experiments reveal similar drying regimes at different concentrations but the formation of two types of patterns.

2. Experimental setup

In the experiments, droplets were evaporated in a Jacomex 314 liter G-Box-T2 glovebox with the humidity regulated within the range of 13–85% (Fig. 1). The nano-particles were iso-density with the fluid; hence, the volumetric and mass concentrations were identical. Nine different nanofluid concentrations were investigated: 0.01%, 0.05%, 0.11%, 0.23%, 0.47%, 1.15%, 2.30%, 4.80% and 5.70%. Experiments were performed at atmospheric pressure $Pa = 1014 \pm 5$ hPa. Room temperature and pressure are recorded by a Lufft weather station (see Brutin et al. 2011 [13] for more details).

The nanofluids used were obtained from Invitrogen(R) for their stability, homogeneity in size and chemical potential (sample F8787). The solutions were stable due to the presence of carboxylate surface functional groups on the surface of the nano-particles. The solvent matrix was water, with 2.30% ± 0.03% in mass, and

contained 24-nm-diameter nano-particles. Solutions of various concentration were obtained by the dilution (lower concentrations) or evaporation (higher concentrations) of a 2.30% original sample. Dilution was performed using distilled water (Bioblock) by weighing the samples. The accuracy of the electronic balance was 10 μg. For 10 mL samples, this accuracy led to an uncertainty due to the dilution or evaporation of less than 0.01%. Thus, the uncertainty in the concentrations was assumed to be equal to the original sample concentration: 0.03%. Droplets with a constant volume of 7 μL were created using an electronic syringe (Eppendorf X-Stream) in all experiments. The droplets were then gently laid down on the substrate.

The variation in drop mass was recorded using a Mettler Toledo XS 105 balance. The balance resolution was 10 μg, which enabled us to weigh samples with masses of up to 81 g. The drop masses investigated were typically 7 mg. The mass signal was recorded on a computer at 10 Hz. Image analysis was performed using a digital camera Canon EOS 7D coupled with a 1–5× macro lens

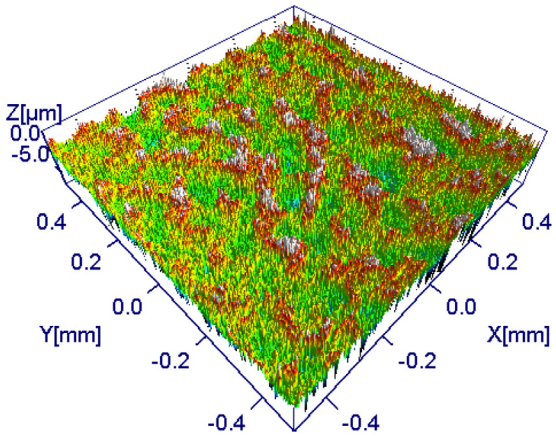

Fig. 2. Surface roughness using a confocal microscope (STILL Micromesure 2). Average standard roughness of 1.736 μm.

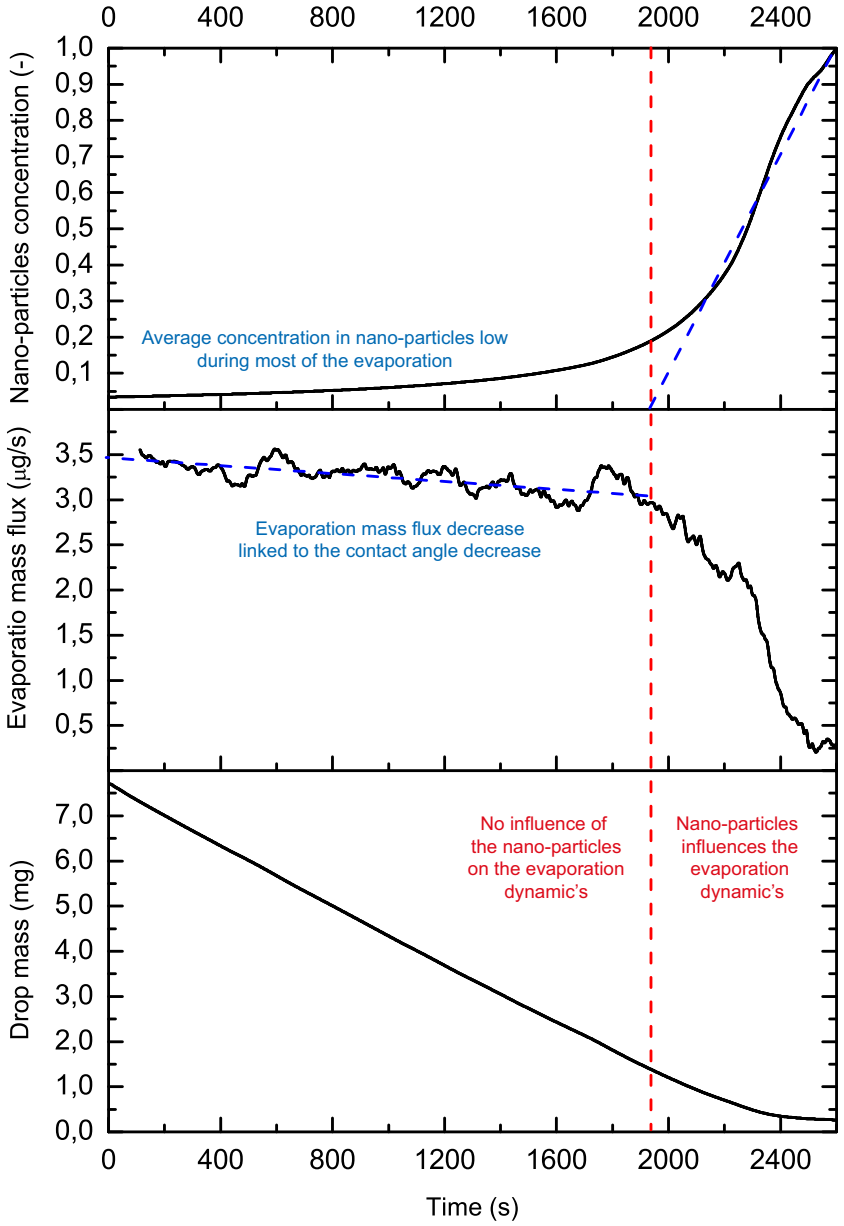

Fig. 3. Mass evolution (bottom figure), evaporation mass flux (middle figure) and mean solid concentration (top figure) as a function of time for a nanofluid concentration of 4.8% at a room humidity of 50%. Two stages of evaporation can be noticed depending on the mass flow rate of evaporation: one when the evaporation mass flux decreases linearly and the other when the evaporation mass flux sharply decrease.

at 0.1 Hz. This camera allowed us to obtain images measuring 5184 × 3456 pixels over an area measuring 22.3 mm ×14.9 mm. At the 1× magnification, the resolution was 4.30 μm, and at the greatest magnification of 5×, the resolution was 0.86 μm. This optical set-up allowed for the visualization of drops from above with enough detail to further analyze specific areas. Illumination was provided by a cold cathode back light at 5000 ± 270 K, without any surrounding light to minimize the reflection at the drop interface.

The substrate was an aluminum disk measuring 10 mm in diameter and 0.5 mm in thickness. A 20–30 μm layer of Nuflon 16× was deposited on the substrate by chemical vapor deposition (APS Coating, Bordeaux, France). The surface roughness was characterized using a confocal microscope (STILL Micromesure 2); an average standard roughness of 1.736 μm was measured (Fig. 2).

The interaction between the Nuflon 16× layer and the water used as the matrix of the nanofluid allowed for the formation of a pinned triple line during evaporation. A typical contact angle of 70° was obtained. Detailed values are provided in Tables 2 and 3. The radii of the all of the droplets were below the capillary length (2.7 mm for pure water) to ensure the formation of a spherical cap at the drop interface (Eq. (1) where R is the wetting radius, θ is the contact angle and V is the sessile droplet volume). Thus, the initial contact angles were calculated from the volume and wetting diameter. In this study, a quasi-steady-state assumption could be made because $Cv(1-H) \ll \varrho$; thus, the diffusion time was far shorter than the characteristic time of evaporation.

$$V(R,\theta) = \frac{\pi R^3}{3} \frac{(1-\cos\theta)^2(2+\cos\theta)}{\sin^3\theta} \quad (1)$$

3. Drying dynamics of a drop of nanofluid

For all experiments, geometrical and physical characteristics were measured, including the initial drop mass m_0, the final drop mass m_F, the initial wetting diameter d and the total time of drying t_F. The characteristic masses and times were obtained from the variation in the droplet mass recorded by the electronic balance, as illustrated in Fig. 3. The total time of evaporation t_F is defined by $m_F(t) = 0$ as dm/dt tends to 0. The uncertainty in the initial drop mass m_0 is 0.1 mg, that in the total time of evaporation t_F is 50 s and that in the radii R_E and R_I is 2.2% based on the image analysis.

From the mass evolution $m(t)$, we can derive the evaporation mass flux and the average solid concentration. The evaporation mass flux clearly shows a drying transition regime immediately below 2000 s, with a transition from a linearly decreasing evaporation mass flux to a sharply decreasing mass flux. At the same time, the mean solid concentration sharply increases. The first regime, with a mean nano-particle concentration below 20%, is very similar to that of the evaporation of a pure fluid drop with a receding triple line (thus a decreasing evaporation mass flux). The transition regime observed for concentrations above 20% is clearly affected by the presence of nano-particles, which slow down the evaporation kinetics.

4. Influence of the surface roughness on the patterns

To compare the total volume of nano-particles in a droplet with the volume of the cavities in the substrate based on a roughness of 1.736 μm, we assume that the substrate roughness can be modeled by tetrahedral cavities. We show that the rough substrate rapidly becomes smooth due to the deposition of nano-particles in the substrate cavities, which fill the empty spaces, using only a few percent of the nano-particles available (see Fig. 4).

We assume that the spherical nano-particles measure 24 nm in diameter and that the initial drop volume is 7 μL. The cavities are

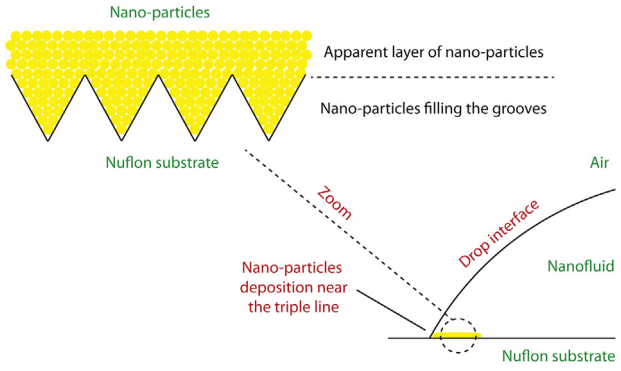

Fig. 4. Nano-particle deposition in substrate grooves.

tetrahedral pyramids measuring 1.736 μm on each side. Thus, each cavity has a volume of 5.79×10^{-19} m^3 and can store 1.21×10^5 nano-particles. The fluid density is 1050 kg/m^3. The tetrahedral cavities are uniformly and continuously distributed over the substrate; thus, we compute the number of nano-particles stored in a cavity based on a compact arrangement (66%). Table 1 shows the percentage of nano-particles stored in the cavities compared to the total number of nano-particles in the droplet.

The number of nano-particles stored inside the cavities of the rough surface is extremely small compared to the total number of nano-particles. For the lowest concentration, only 0.81% of the nano-particles are deposited in the cavities, while 99.19% is deposited above the cavities. Consequently, we can conclude that immediately after drop deposition, the external periphery of the substrate beneath the drop is covered with nano-particles. Thus, pattern formation is not affected by a surface roughness of 1.736 μm.

5. Influence of nanofluid concentration on drying and pattern formation

5.1. Drying and pattern formation

Experiments were performed by varying the concentration of the nanofluids at a constant glovebox humidity of 50%. Drops of a given mass were weighed and controlled initially; the initial dispersion in drops with a mass of 7 mg ± was 6.0%. The measured room temperature was a nearly constant 25.0 °C ± 0.6 °C. Because the experiments were carried out over several days, the atmospheric pressure slightly varied, 1013.4 hPa ± 4.9 hPa. All of the drops had an initial contact angle of 67.5° ± 8.1%, as illustrated in Table 2 where m_0 is the drop mass, t_F is the time of drying, R are the external

Table 1
Amount of nano-particles in a 7 μL droplet, depending on the concentration, deposited on a substrate cavities. Percentage of nano-particles in the cavities and apparent layer above the cavities. The three highest concentrations show a uniform deposition of the nano-particles, while the others show the formation of an o-ring; this last area of deposition is consequently much smaller [NP: nano-particles].

ϕ (%)	Number of NP (−)	Area covered by cavities (mm^2)	Number of cavities below the deposit	NP in cavities % of total
5.7	5.25E+15	10.752	8.59E+06	0.02
4.8	4.42E+15	12.316	9.84E+06	0.03
2.3	2.12E+15	9.186	7.34E+06	0.04
1.15	1.06E+15	2.852	2.28E+06	0.03
0.47	4.33E+14	2.212	1.77E+06	0.05
0.23	2.12E+14	2.187	1.75E+06	0.10
0.11	1.01E+14	1.575	1.26E+06	0.15
0.05	4.61E+13	1.185	9.47E+05	0.25
0.01	9.21E+12	0.767	6.13E+05	0.81

Table 2
Set of experiments conducted at constant humidity of 50% for different nanofluid concentrations ranging from 0.01% to 5.70%. J^*_{model} was obtained based on a purely diffusive model [15].

ϕ (%)	m_0 (mg)	t_F (s)	R_E (mm)	R_I (mm)	w/r_E (−)	J^*_{exp} (mg s^{-1} m^{-1})	J^*_{model} (mg s^{-1} m^{-1})	θ(°)
5.70	7.4	2350	1.85	–	–	1.70	1.30	66.2
4.80	7.7	2450	1.98	–	–	1.70	1.27	59.2
2.30	7.4	2600	1.71	–	–	1.66	1.34	75.9
1.15	7.0	2250	1.71	1.42	0.169	1.82	1.06	73.6
0.47	6.4	2600	1.71	1.49	0.129	1.44	1.32	70.4
0.23	7.0	2600	1.84	1.64	0.104	1.50	1.30	65.0
0.11	6.7	2350	1.86	1.72	0.075	1.50	1.28	61.1
0.05	6.6	2200	1.77	1.66	0.064	1.73	1.30	66.9
0.01	7.1	2350	1.78	1.71	0.039	1.74	1.32	69.6

and internal droplet radii when applicable, w is the corona width, J^*_{exp} is the evaporation mass flux per drop radius length $2m_0/(t_F d_E)$.

The evaporation of the nanofluid drops led to the formation of certain patterns, as shown in Fig. 5. For concentrations below 1.15%, the drops formed an o-ring shape whose width decreased with concentration. This o-ring formation was previously observed by Deegan [9] using a 2% mass concentration of sulfate-terminated polystyrene microspheres dyed yellow–green with diameters of 1 and 0.1 μm. However, the author did not investigate the effect of the concentration on the ring formation. In our study, experiments using particle concentrations below 0.01% were not performed because the uncertainty in the concentration was too significant and because the measured width was not accurate.

Two main types of patterns could be observed as a function of the concentration:

- From 0.01% to 0.47%, the drops formed an o-ring pattern with no particles at the center. The width of the deposits was observed to decrease. No nano-particles were detected at the drop center.

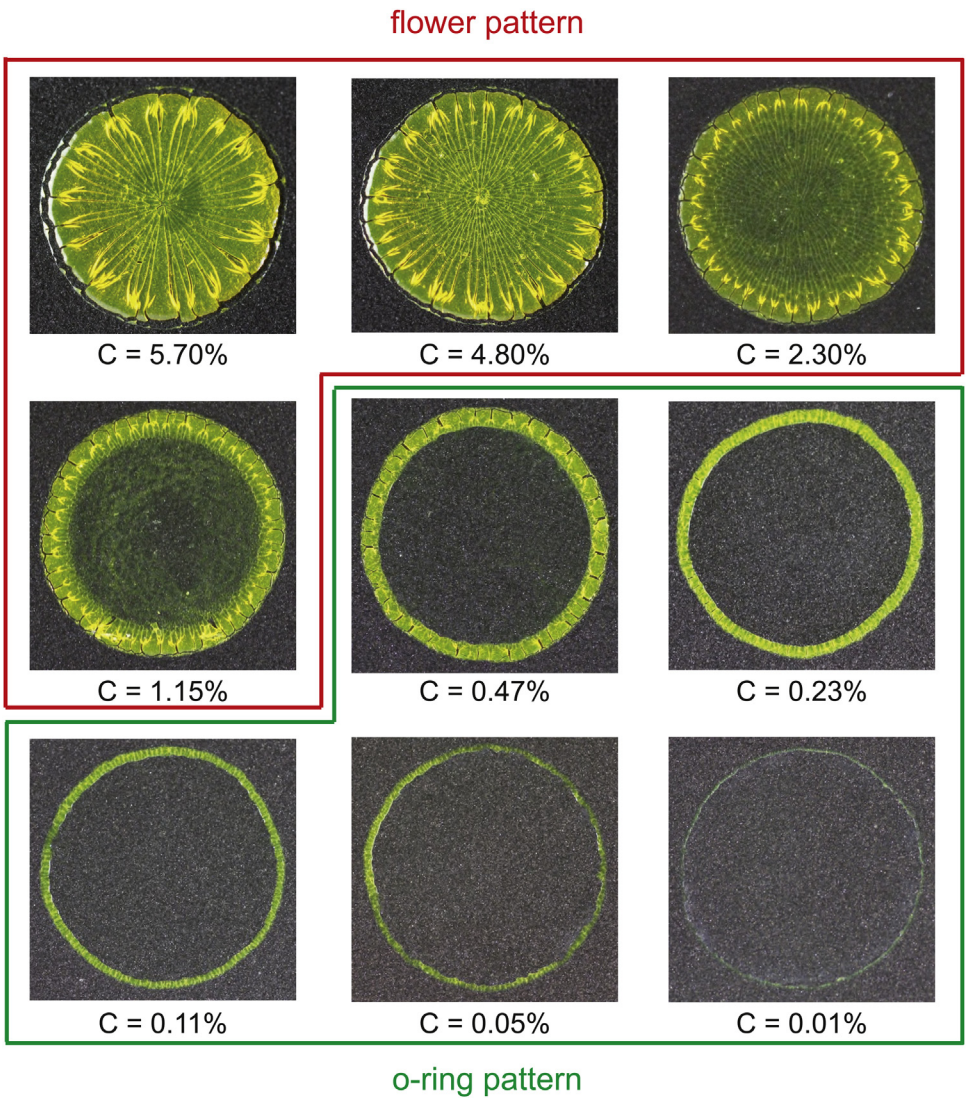

Fig. 5. Influence of nanofluid concentrations ranging from 0.01% to 5.70% on pattern formation (glovebox humidity of 50%, room temperature of 25.0 °C ± 0.6 °C).

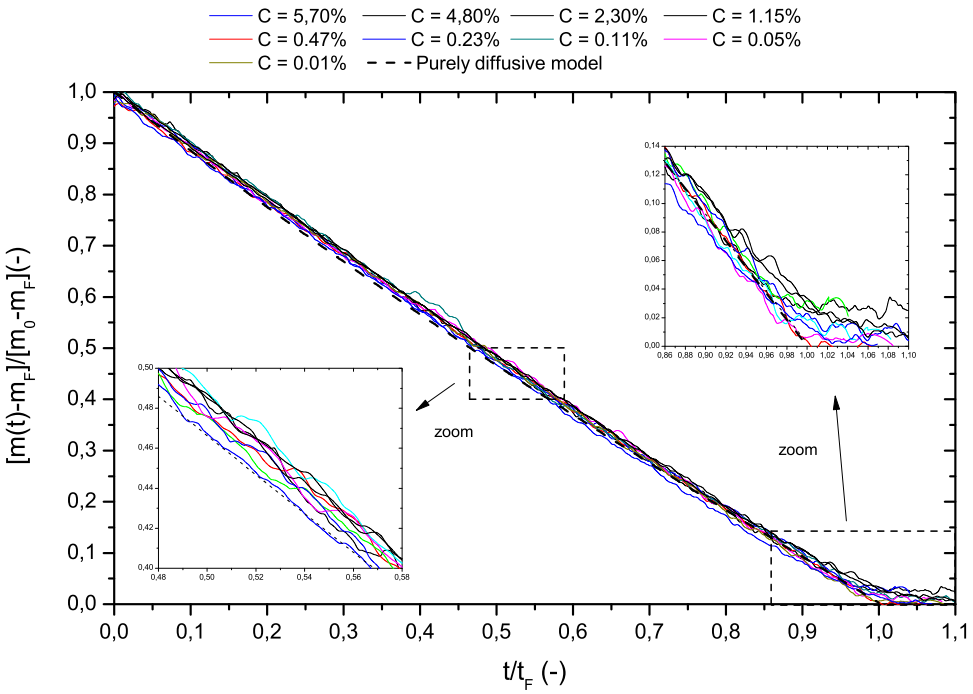

Fig. 6. Normalized mass variation as a function of normalized time for nanofluid concentrations ranging from 0.01% to 5.70% (room humidity of 50%). The inset is a magnification of t/t_D from 0.85 to 1.10 that illustrates the effect of the concentration on the final stage of drying. The dashed line is Eq. (2).

All nano-particles were deposited along the o-ring, whose width decreased with the nanofluid concentration.

- For concentrations of 1.15% and above, particles were deposited at the center of the drop and the deposition thickness increased with concentration. The formation of an axisymmetric flower petal pattern was clearly observed. Several patterns were noted. The number of flower petals decrease with increasing concentration. The final diameter also decreased due to a clear retraction of the drying edge.

At constant humidity, the evaporation mass flux was 1.60 μg/(s mm) ± 8.0%, with an average experimental uncertainty of 5.6%, for concentrations ranging from 0.01% to 5.70%. The overall evaporation rate was higher than that obtained with a purely diffusive model, following Eq. (2), for which an approximation of $f(\theta)$ is provided by Hu and Larson [17]. The experimental droplet radii and initial contact angles were substituted into the model to determine the total time of evaporation and consequently the evaporation rate. The quasi-steady diffusion evaporation mass flux was 1.28 μg/(s mm) ± 6.6%, which is within the uncertainty of the experimental measurements. The experimental evaporation rates were 25% higher than those predicted by the model. These parameters were also studied at a fixed concentration and different levels of humidity for verification.

$$-\frac{dm}{dt} = \pi R D c_v (1 - H) f_{HL}(\theta) \quad (2)$$

$$f_{HL}(\theta) = 1.3 + 0.27\theta^2 \quad (3)$$

5.2. Drying dynamics

Fig. 6 presents the normalized mass $[m/m_0]$ as a function of the normalized time $[t/t_D]$ using the diffusion times and initial drop mass. The dashed line represents a constant evaporation mass flux based on Eq. (2). Because the drop contact angle decreased from approximately 70° to 0, the contact angle function f_{HL} varies between 1.7 and 1.3. This induces a slightly nonlinear variation in the normalized mass over time.

All experimental mass curves collapse, indicating that the concentration does not disturb the evaporation dynamics, except during the last step of the evaporation process. Indeed, as shown in the inset of Fig. 6, the concentration plays a role in the evolution of the drops only during the last few stages of drying. This result indicates that, for all concentrations, the main stages of droplet evaporation are not affected by the nanofluid concentration, while at the end of evaporation, when the local concentration is important, the concentration plays an important role. Depending on the initial concentration, either an o-ring will form or nano-particles will be deposited at the center of a drop (see Fig. 5).

5.3. Variation in o-ring width

For our 24-nm-diameter nano-particles, a critical concentration occurs between 0.47% and 1.15%. Below 0.47%, only o-ring patterns are formed, while above 1.15%, nano-particles deposit at the center of drying drops (see Fig. 5). Both patterns can be quantitatively characterized. The o-ring pattern is characterized by its width, which decreases with the concentration following a power law, as evidenced in Fig. 7. This power law behavior is explained by the effect of the nano-particles on the triple line behavior during the last stages of evaporation. Nano-particles accumulate near the triple line during the first 80% of the evaporation time; then, the triple line recedes due to the deepening effect reported by previous authors for such cases [1].

The ring width can be related to the concentration by the power law correlation: $w/r = \alpha C^{\beta}$ with $\alpha = 1.72 \pm 1.92\%$ and $\beta = 0.346 \pm 4.23\%$. In 2000, R. Deegan obtained similar patterns with microspheres measuring 0.1 and 1 μm and also observed power law behavior. However, his power law exponent β was 0.78 ± 12.8% for 0.1 μm-diameter microspheres and 0.86 ± 11.6% for 1 μm-diameter microspheres. In our case, using nano-particles measuring 24 nm in diameter, the value $\beta = 0.346 \pm 4.23\%$ is consistent even if no quantitative link can be made between these values

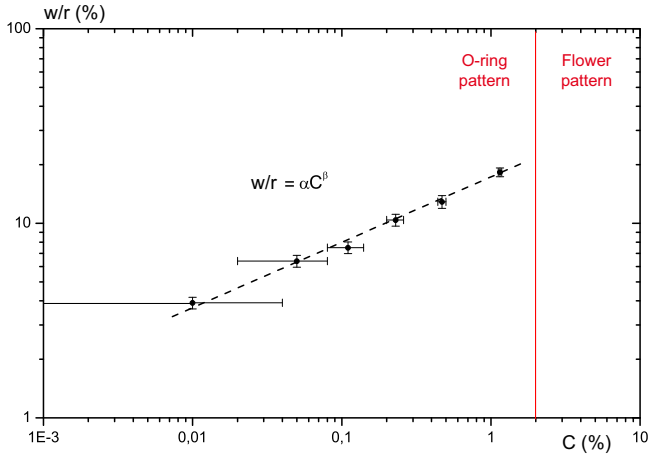

Fig. 7. Dimensionless o-ring width $[w/r]$ as a function of the nanofluid concentration (constant room humidity of 50%). $w/r = \alpha C^{\beta}$ with $\alpha = 1.72 \pm 1.92\%$ and $\beta = 0.346 \pm 4.23\%$.

for micro- and nano-particles. Our nano-particles were coated with carboxylate (Invitrogen F8787), while the microspheres used in Deegan's study were not. In a future study, we will vary the nano-particle size to investigate the effect on β.

6. Influence of humidity on drying and pattern formation

6.1. Drying and pattern formation

Experiments were performed by varying the humidity in the glovebox between 13% and 85%. The same initial mass of 7 mg ± 4.8% was weighed over time. See Table 3 for a summary of the relevant droplet characteristics. T is room temperature, which was a nearly constant 24.9 °C ± 0.6 °C, and P is the atmospheric pressure, which was a nearly constant 1013.5 hPa. Because the experiments were carried out over several days, the atmospheric pressure slightly varied, 1013.6 hPa ± 4.8 hPa.

Experiments were performed at a controlled concentration of 1.15%, for which a very thin layer of nano-particles was deposited at the center of the droplets. The initial drop diameter was 3.54 mm ± 3.7%; thus, the initial drop radius was 1.77 mm ± 3.7%. For all drops, the wetting contact angle was 69.6° ± 8%, according to Eq. (1).

Surprisingly, all of the dried drops of the nanofluids led to the same pattern, as shown in Fig. 8. Changing the glovebox humidity greatly altered the total time of evaporation from 23 min at 15% to 112 min at 87%. However, even if the internal flow inside the drops was strongly enhanced, we observed, using Fig. 8, that the final pattern was not modified. The same corona with a thin layer of nano-particles in the central area was observed. The o-ring width of all nine drops was measured to be 23.1% ± 5.6% of the initial diameter. The drops held under different glovebox humidities evaporated with different evaporation mass fluxes, which could be predicted using Eq. (2), but the final pattern was almost exactly the same. The o-rings that formed were 23.1 % ± 5.6% of the initial drop radii for all humidities. This result can be explained by the fact that the mechanism by which the nano-particles are transported to the drop edge is internal convection. The internal flow motion is directly proportional to the evaporative mass flux; consequently, the intensity of evaporation scales with that of internal convection, which transports the nano-particles to the drop perimeter, where they accumulate.

The nano-particles were transported to the droplet edge by internal flow motion. When the humidity was decreased, the global evaporation mass flux increased; thus, at the triple line, the local evaporation mass flux also increased. Therefore, the amount of liquid transported to the triple line consequently increased due to the proportional increase in the internal flow motion. The internal flow motion inside the droplets adapted to the external flow of vapor in the air. Because the nano-particles were carried out by the liquid, the increase in the internal flow velocities enhanced the transportation mechanism pushing nano-particles to the drop edge. Thus, the pattern formation was still the same but was realized more quickly because the mechanism of formation was the same.

Similar flower pattern formation have been observed in high concentration colloidal suspensions such as polymer [20] or even blood [14,19]. The different behaviors are analyzed by the authors using a stability diagram obtained for colloidal suspensions. The same mechanisms could be applied for drops of blood composed of high concentration particles of 8 μm. For these mechanisms encountered in blood, the radial cracks formation is due to a stress release in the dry-out. Due to the solvent evaporation, a closed packed array of colloid is formed and stuck in between two interfaces: substrate–colloids interface and colloids air interface. The solvent evaporation create a pressure onto the colloids–air interface. This stress release periodically depending on the competition between the colloids adhesion onto the substrate and the evaporation rate. The same mechanisms can explain the flower pattern formation due to a stress release in the dry-out. This mechanisms is not possible at low concentration since there is not enough material deposited.

6.2. Drying dynamics

The mass flow rate of evaporation per drop radius is plotted in Fig. 9 and shows an increasing linear trend with decreasing humidity (so increasing $[1 - H]$). A purely diffusive model using 2 also shows a linear trend but with a lower slope compared to that of the experimental results.

For pure fluids, such as water, under the same conditions of substrate wettability, temperature and humidity without the heating of the substrate, a purely diffusive model was used to fit the data. We observe in the slopes α a difference of 24% with a higher experimental evaporative mass flux compared to that of the pure fluid. When the evaporation was slow for $(1 - H)$ small, the difference

Table 3
Set of experiments performed at a constant nanofluid concentration of 1.15% at different humidities ranging from 13% to 85%.

H (%)	m_0 (mg)	t_F (s)	R_E (mm)	R_I (mm)	w/R_E (−)	J^*_{exp} (mg s^{-1} m^{-1})	J^*_{model} (mg s^{-1} m^{-1})	θ (°)	T (°C)	P (hPa)
13.0	7.0	1400	1.77	1.39	0.214	2.82	2.26	69.4	24.9	1019.0
20.0	7.2	1600	1.74	1.35	0.225	2.59	2.20	72.9	25.6	1018.6
30.0	6.7	1800	1.67	1.26	0.248	2.23	1.95	74.9	25.8	1018.6
41.0	7.8	2250	1.68	1.29	0.237	2.05	1.57	80.0	24.5	1008.7
50.0	7.0	2400	1.78	1.38	0.227	1.64	1.31	68.7	25.0	1013.1
60.5	6.9	2700	1.79	1.40	0.220	1.42	0.96	67.2	23.8	1004.7
70.0	7.3	3750	1.85	1.45	0.218	1.04	0.78	65.1	25.0	1013.1
78.0	6.7	4800	1.78	1.35	0.243	0.78	0.57	66.9	25.0	1013.1
85.0	6.8	6750	1.87	1.41	0.246	0.54	0.38	61.4	24.9	1012.2

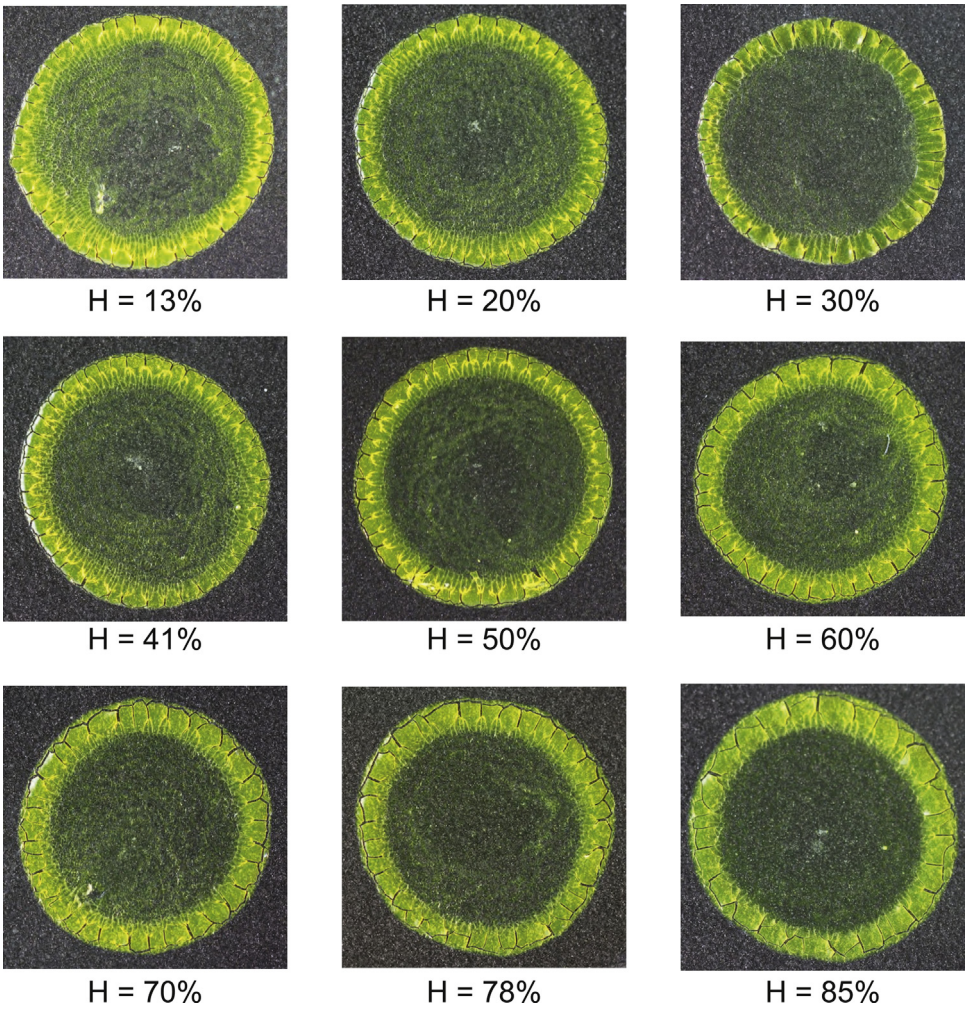

Fig. 8. Influence of humidity ranging from 15 to 87% on pattern formation (nanofluid concentration of 1.15%).

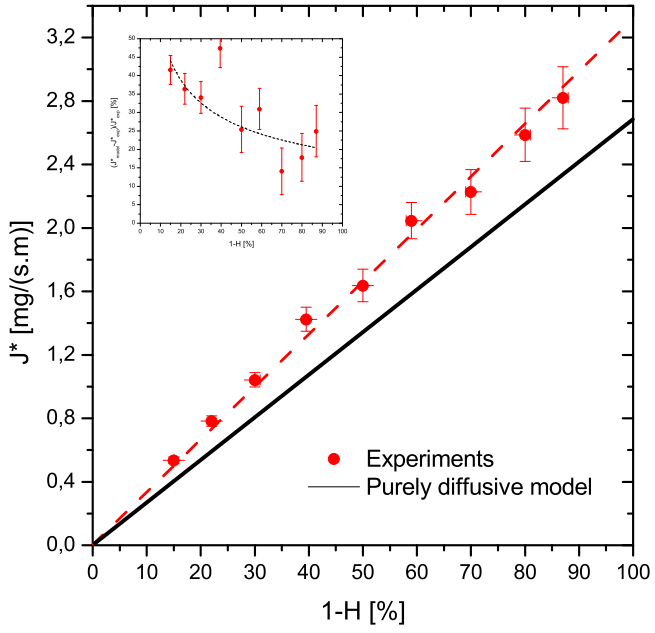

Fig. 9. Evaporation mass flow rate per drop radius as a function of the $[1 - H]$ for the same nanofluids with a concentration of 1.15%. The experimental results were compared to those of a purely diffusive model based on Eq. (2). Linear evolution of both J^* with $J^* = \alpha(1 - H)$ with $\alpha_{exp} = 3297\ \mathrm{mg\,s^{-1}\,m^{-1}} \pm 1.35\%$ and $\alpha_{model} = 2664\ \mathrm{mg\,s^{-1}\,m^{-1}} \pm 1.27\%$.

was small in terms of $\mathrm{mg\,s^{-1}\,m^{-1}}$. However, when the evaporation was five times faster (ratio of evaporation rates at 13% humidity compared to that at 85% humidity), a gap was clearly observed.

The experiments reported in the literature have rarely been performed at high relative humidity, considering the longer period over which such experiments were carried out. Additionally, in most research laboratories, air conditioning controls the relative humidity to be approximately 50% to limit bacteria propagation at high RH and to prevent throat pains at lower RH. It is very likely that, in the literature, such experimental results are assumed to be in agreement with a purely diffusive model if the authors cannot provide results with small uncertainty. With our relatively very low uncertainties, we are able to show that such a difference seems to be nearly constant, approximately 24% ± 2.62%. The explanation for this difference should be investigated by studying the diffusion coefficient of our nanofluids in humid air, which is based on the evaporation of pure water in dry air. Complementary experiments should confirm our assumptions.

Another possible explanation proposed is based on the effect of relative humidity on spreading. Chhasatia and Sun [1] reported an increase in spreading and a decrease in the initial contact angle with increasing relative humidity for pico-liter droplets of a water-based nanofluid. The nanofluids used in this study are the same as those used by Chhasatia et al. If we assume the same behavior, then even a slight increase in spreading coupled with a slight decrease in the contact angle would induce a higher evaporation rate. Our diffusive model presented in Fig. 9 is based on the initial droplet

contact angle and does not take into account the change in the droplet contact angle during the evaporation process. The effects of the increase in spreading could be more significant throughout the entire evaporation process. This assumption is currently being tested by monitoring the entire evaporation process to compute the drop diameter and contact angle at all times.

7. Conclusions

Polystyrene nano-particles measuring 24 nm were suspended in deionized water to study the effect of nano-particle concentration and surrounding humidity on the pattern formation and drying dynamics of sessile droplets. Droplets were deposited on rough Nuflon 16×-coated substrates. The patterns formed were observed to have been influenced mainly by the concentration of nano-particles but not at all by the drying time. Two patterns were observed: an o-ring formation for concentrations below 0.47% and a flower pattern above 1.15%. The effect of humidity was proportional to the drying rate, but no effect on pattern formation was observed. The experimentally measured evaporative mass flux was slightly higher compared to that predicted by a purely diffusive model, which may indicate a slight enhancement in heat transfer at the triple line due to the local improvement in the substrate heat capacity by nano-particle deposition.

For pure fluids, the effect of the substrates thermal properties was investigated, even at ambient temperature, because the latent heat of evaporation is mostly affected by element with the highest heat capacity, which is the substrate [21]. One explanation is that the diffusion coefficient of our water-based nanofluid, even at low concentration, in humid air is different from that of pure water in dry air. Experiments are currently underway to address this discrepancy. Another explanation is based on the experimental observation in the literature of an increase in the spreading of nanofluids leading to an increase in the drop perimeter and a simultaneous decrease in the contact angle. The consequence is an improvement in the evaporation rate. This assumption is also under investigation at this time.

Acknowledgements

The author thanks the Carnot STAR for the financial support provided through the NanoPhaseChange Project. The author is also grateful to F. Martinez and B. Sobac for their fruitful discussions and participation.

References

[1] V.H. Chhasatia, Y. Sun, Interaction of bi-dispersed particles with contact line in an evaporating colloidal drop, Soft Matter 7 (2011) 10135–10143.
[2] J. Barber, D. Brutin, L. Tadrist, A review on boiling heat transfer enhancement with nanofluids, Nanoscale Res. Lett. 6 (2011) 1–16.
[3] A. Askounis, K. Sefiane, V. Koutsos, M.E.R. Shanahan, The effect of evaporation kinetics on nanoparticle structuring within contact line deposits of volatile drops, Colloids Surf. A, http://dx.doi.org/10.1016/j.colsurfa.2012.10.017, in press.
[4] S. David, K. Sefiane, L. Tadrist, Experimental investigation of the effect of thermal properties of the substrate in the wetting and evaporation of sessile drops, Colloids Surf. A 298 (2007) 108–114.
[5] P.L. Kelly-Zion, C.J. Pursell, S. Vaidya, J. Batra, Evaporation of sessile drops under combined diffusion and natural convection, Colloids Surf. A 381 (2011) 31–36.
[6] V. Starov, K. Sefiane, On evaporation rate and interfacial temperature of volatile sessile drops, Colloids Surf. A 333 (2009) 170–174.
[7] J. Conway, H. Korns, M.R. Fish, Evaporation kinematics of polystyrene bead suspensions, Langmuir 13 (1997) 426–431.
[8] A. Marin, H. Gelderblom, D. Lohse, J.H. Snoeijer, Order-to-disorder transition in ring-shaped colloidal stains, Phys. Rev. L (2011) 085502.
[9] R.D. Deegan, Pattern formation in drying drops, Phys. Rev. E 61 (2000) 475–485.
[10] V.H. Chhasatia, A.S. Joshi, Y. Sun, Effect of relative humidity on contact angle and particle deposition morphology of an evaporating colloidal drop, Appl. Phys. Lett. 97 (2010) 231909.
[11] L.V. Govor, G. Reiter, G.H. Bauer, J. Parisi, Nanoparticles ring formation in evaporating micro-size droplets, App. Phys. Lett. 84 (23) (2004) 4774–4776.
[12] D. Brutin, B. Sobac, F. Rigollet, C. Le Niliot, Infrared visualization of thermal motion inside a sessile drop deposited onto a heated surface, Exp. Therm. Fluid Sci. 35 (2011) 521–530.
[13] D. Brutin, B. Sobac, B. Loquet, J. Sampol, Pattern formation in drying drops of blood, J. Fluid Mech. 667 (2011) 85–95.
[14] B. Sobac, D. Brutin, Structural and evaporative evolutions in desiccating sessile drops of blood, Phys. Rev. E 84 (2011) 011603.
[15] B. Sobac, D. Brutin, Triple-line behavior and wettability controlled by nanocoated substrates: influence on sessile drop evaporation, Langmuir 27 (2011) 14999–15007.
[17] H. Hu, R. Larson, Evaporation of a sessile droplet on a substrate, J. Phys. Chem. B 106 (2002) 1334–1344.
[18] C. Monteux, F. Lequeux, Packing and sorting colloids at the contact line of a drying drop, Langmuir 27 (2011) 2917–2922.
[19] D. Brutin, B. Sobac, C. Nicloux, Influence of substrate nature on the evaporation of a sessile drop of blood, J. Heat Transfer 134 (2012) 061101.
[20] L. Pauchard, C. Allain, Stable and unstable surface evolution during the drying of a polymer solution drop, Phys. Rev. E 68 (2003) 052801.
[21] B. Sobac, D. Brutin, Thermal effects of the substrate on water droplet evaporation, Phys. Rev. E 86 (2012) 021602.
[22] N. Denkov, O. Velev, P. Kralchevski, I. Ivanov, H. Yoshimura, K. Nagayama, Mechanism of formation of two-dimensional crystals from latex particles on substrates, Langmuir 8 (12) (1992).